minerals

Article

Integration of Seismic Refraction and Fracture-Induced Electromagnetic Radiation Methods to Assess the Stability of the Roof in Mine-Workings

Sergei Daniliev [1], Natali Danilieva [1], Sergei Mulev [2] and Vladimir Frid [3,*]

[1] Department of Geophysics, The Faculty of Geological Exploration, Saint Petersburg Mining University, 21lin. 2, VO, 199106 Saint Petersburg, Russia; danilev_sm@pers.spmi.ru (S.D.); danileva_na@pers.spmi.ru (N.D.)
[2] JSC VNIMI, 3A, 21 Lin., V.O., 199106 Saint Petersburg, Russia; smuleva@yandex.ru
[3] Sami Shamoon College of Engineering, Jabotinsky 84, Ashdod 77245, Israel
* Correspondence: vladimirf@ac.sce.ac.il

Abstract: This paper considers the joint use of two popular geophysical methods (fracture-induced electromagnetic radiation and seismic refraction tomography) to assess the stress-state in underground mine-workings. Such a combination of two indirect methods allows the identification of zones of increased stress in the rock along the axis of the mine-workings, and zones of intense weakening or disintegration in the rock massif above the roof of the mine-workings. The measurements of longitudinal and compressive wave speeds were used to calculate 2D sections of Young's modulus and Poisson's ratio to assess the rock mechanical properties in the vicinity of the mine-workings. It is shown that the anomalies of both elastic parameters correspond to those of fracture-induced electromagnetic radiation.

Keywords: underground mining; rock stress assessment; fracture induced electromagnetic radiation; seismic refraction

check for updates

Citation: Daniliev, S.; Danilieva, N.; Mulev, S.; Frid, V. Integration of Seismic Refraction and Fracture-Induced Electromagnetic Radiation Methods to Assess the Stability of the Roof in Mine-Workings. *Minerals* **2022**, *12*, 609. https://doi.org/10.3390/min12050609

Academic Editors: Anye Cao and Zhenlei Li

Received: 7 April 2022
Accepted: 6 May 2022
Published: 12 May 2022

Publisher's Note: MDPI stays neutral with regard to jurisdictional claims in published maps and institutional affiliations.

1. Introduction

1.1. Geological Background

The Norilsk Mining and Metallurgical Company is the largest mining enterprise engaged in extracting, enriching and processing copper-nickel ores. It operates three main deposits of rich, cuprous, and disseminated copper-nickel ores, the origin, structure, and properties of which have been studied in detail [1–7]. The value of uniaxial compression strength of the rocks is of the order of 80–160 MPa, the tension and shear strength values range from 10–16 MPa and 4–5 MPa, respectively, while the values of Young's modulus, Poisson's ratio, density and the angle of internal friction are 80–85 GPa, 0.19–0.25, 3000 kg/m^3, and 33–38°, respectively [8].

The deposits have been developed over decades in several underground mines, at depths ~500–2000 m below the Earth's surface, as well as close to the permafrost surface [9–11].

Ore mining at deep horizons is inevitably accompanied by an increase in rock pressure, which often causes the failure of rocks in a dynamic form (e.g., in the form of rockburst). Underground mining in the Norilsk region involves working in permafrost [7], leading to the degradation of permafrost zones and, as a result, to the loss of rock bearing capacity, and the formation of channels of water inflow from the upper aquifers, rock/soil subsidence, sinkhole formation, etc. [12,13].

The possibility of dangerous mining phenomena occurring, and the stability of underground excavations and structures on the Earth's surface, are assessed via changes in the stress-strain state of rocks [14–17]. The increase in stress levels during mining causes the development of rock fractures and, consequently, the appearance of areas of significant weakening of rocks, followed by their failure. The regions of rock fracturing are sources of increased water inflow towards underground excavations.

In the mines of Norilsk, the complex of geotechnical monitoring works traditionally consists of surveying observations against benchmarks, monitoring of seismic events within the seismic pavilions of the mines, and hydrogeological monitoring (e.g., [9–11,18–21]).

It is known that the formation of micro-cracks precedes the appearance of visible macro-fractures and hence heralds potentially significant changes in the state of stress [22–24]. Underground geophysical methods have been successfully used for more than half a century [22–29] to assess the rock micro-fracturing and the stress-state of rocks near the mine-workings.

1.2. Geophysical Methods in Mining

There are no essential differences between the application of conventional geophysical methods and their use in underground conditions (e.g., [25,26,30–35]). However, the goals of their application, and the methodologies of data processing and interpretation have specific peculiarities. The main goal of the application of underground geophysical methods is to assess the stress-state of rocks. Experience shows that the most frequently used methods are seismic refraction (SRfr) and reflection (SRfl) methods, borehole ultrasonic and seismic methods, direct current and transient electromagnetic methods, acoustic emission, and fracture-induced electromagnetic radiation (FEMR) [35–59]. These methods can be used to simplify and intensify the assessment of roof and wall stability in underground excavations, and to reduce rock disintegration during the examination process.

The high-resolution seismic-reflection method has been used for the evaluation of rock subsidence associated with underground mining [36,37] and for roof stability assessment [38]. The method was shown to be useful for the analysis of rock stratification and disintegration at tens of meters from seismic sources. Note that seismological and seismic-acoustic measurements are often employed in underground mining for the assessment of rock-burst hazards [22,39–45].

Micro-seismic (acoustic emission) monitoring is a useful and often mandatory tool for stress-state assessment, especially in rock-burst and rock- or gas-outburst-prone mines [20,21,46]. However, since the frequency of elastic signals is relatively low, seismic-acoustic activity is associated with quite large fractures [24,47], and hence it is used for stress-state assessment across the entire minefield or in its larger areas.

Electrical resistivity tomography has been shown to be especially useful for detecting zones of intensive fracturing (which can be sources of gas outflow and/or water inflow to excavations) [48], as well as for delineating and mapping water and cavities [49].

The SRfr method has been used to discover areas of high vertical stress in the roof of underground excavations [50] and to assess their stability [51]. The approach is based on the relationship between the stress level and the P- and S-velocities in rocks, and enables one to distinguish between high, medium, and low-stress levels.

Being indirect tools, the above methods can all cause ambiguity in interpretation and, so, in decision-making. To avoid such a problem, the integration of a pair or more of these geophysical methods is preferable for use. However, despite its actual advantages, this approach is time-consuming and often expensive, so such studies are rarely undertaken.

The integration of two geophysical methods (FEMR and SRfr) employed for the stress-state assessment of mine-workings is the subject of the study presented in this article.

2. Methods and Instruments

An integration of FEMR and SRfr methods was used to study roof stability in underground mine-workings.

2.1. FEMR Methods and Instrument

FEMR measurements in mine-workings were conducted with the ANGEL-M instrument manufactured by JSC VNIMI (St. Petersburg, Russia). It was developed specifically for FEMR measurements in mine-workings and underground tunnels, as well as on the Earth's surface, to detect stress directions near tectonic faults and landslides (see the series of studies (e.g., [58–65])). The assemblage of the instrument consists of a registration/control unit and a receiving electromagnetic antenna (loop or whip antennae can be used). The device automatically receives FEMR pulses induced by rock micro-fracturing. Figure 1 shows the use of the Angel-M instrument for FEMR measurement in an underground mine deposit in Norilsk, aiming to assess the state of stress in the rock around the underground excavation. The fixed direction of radiation reception was set by the orientation of the antenna. One operator was sufficient for field observations using the instrument (Figure 1). The measurement results were displayed on the instrument panel, where the hit/pulse number and the values of two parameters (A- and B-factors) were indicated; where the A-factor was the average amplitude of the pulses recorded in each time interval (10, 20, 40 or 80 s), B-factor (the slope of the relationship between the number of FEMR pulses and their amplitude) showed (in accordance with the Gutenberg-Richter relationship) a distribution of pulse amplitudes over 10 levels. The measured parameters were recorded in the instrument's memory for later download to a PC for further filtering and processing [64,65]. Figure 2 portrays two examples of data presentation registered using the Angel-M device.

Figure 1. The use of Angel-M device for FEMR measurement in the Norilsk underground mine.

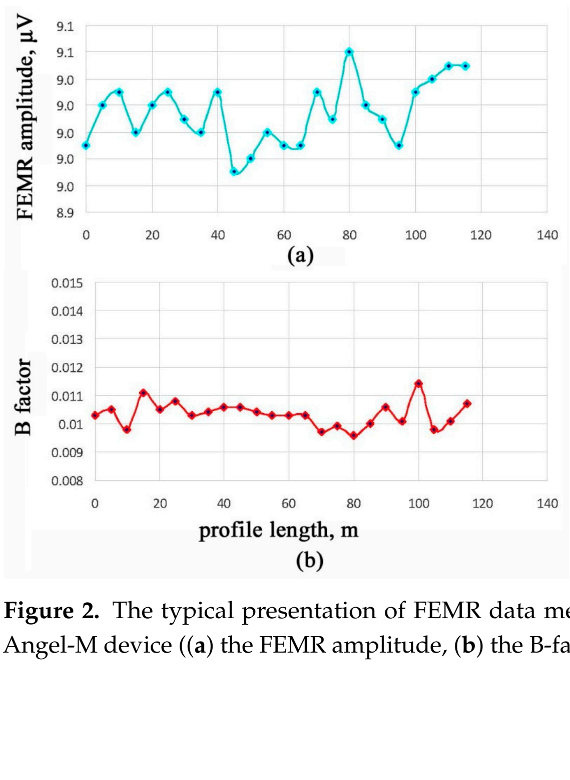

Figure 2. The typical presentation of FEMR data measured in an underground tunnel using the Angel-M device ((**a**) the FEMR amplitude, (**b**) the B-factor values).

The obtained values of A- and B-factors were collected in the FEMR Catalog (the fragment of which is presented in Table 1), which served as the basis for the assessing state of stress.

Table 1. The fragment of the FEMR Catalog used for the stress-state assessment.

Profile Length, m	Profile 2		Profile Length, m	Profile 3		Profile Length, m	Profile 4		Profile Length, m	Profile 5	
	A	B		A	B		A	B		A	B
10	6.25	0.0344	0	7.08	0.0335	20	9.01	0.0091	15	9.01	0.0104
15	6.30	0.0318	5	6.99	0.0316	25	9.03	0.0103	20	9.12	0.0092
20	6.47	0.0325	10	6.55	0.0372	30	9.04	0.0099	25	9.02	0.0097
25	6.33	0.0345	15	6.53	0.0343	35	8.99	0.0100	30	9.01	0.0104
30	6.33	0.0322	20	6.54	0.0318	40	9.11	0.0099	35	9.02	0.0105
35	6.49	0.0343	25	6.13	0.0335	45	8.97	0.0103	40	9.06	0.0100
40	6.26	0.0332	30	6.16	0.0352	50	9.06	0.0102	45	9.05	0.0108
45	6.18	0.0345	35	6.26	0.0332	55	8.96	0.0098	50	9.00	0.0099
50	6.24	0.0316	40	6.32	0.0332	60	9.03	0.0100	55	9.05	0.0109
55	6.23	0.0350	45	6.09	0.0334	65	8.99	0.0107	60	9.05	0.0096
60	6.17	0.0317	50	6.15	0.0356	70	9.05	0.0104	65	9.00	0.0104
65	6.24	0.0347	55	6.20	0.0349	75	9.02	0.0096	70	8.99	0.0100
70	6.26	0.0375	60	6.12	0.0319	80	9.00	0.0112	75	9.04	0.0098
75	6.28	0.0381	65	6.11	0.0337	85	8.98	0.0101	80	9.03	0.0103
80	6.45	0.0324	70	6.16	0.0321	90	9.05	0.0110	85	8.97	0.0105
85	6.43	0.0315	75	6.16	0.0336	95	9.05	0.0086	90	9.02	0.0100
90	6.16	0.0345	80	6.17	0.0330	100	9.01	0.0104	95	9.04	0.0108
95	6.21	0.0337	85	6.26	0.0324	105	9.02	0.0106	100	9.04	0.0101
100	6.27	0.0341	90	6.11	0.0333	110	9.01	0.0097	105	9.02	0.0105
105	6.26	0.0333	95	6.22	0.0334	115	9.01	0.0101	110	9.06	0.0105

Despite the advantages of the FEMR method for the scrutiny of the state of stress in mine-workings, its relative simplicity and efficiency allows assessment of the depth of the zone of increased stress (from the tunnel surface towards the rock massif) and its volume [55,56], but does not allow their correct measurement.

To avoid this restriction, the SRfr method after topographic data processing was integrated with the FEMR method to study the zones with anomalous FEMR measurements.

2.2. *SRfr Method and Instrument Used*

Surveys of SRfr in the FEMR anomalous excitation zone were carried out to estimate the values of Young's modulus and Poisson's ratio. The measurements were performed to a depth of 50 m from the surface of the mine-working. Geophones (seismic sensors) were installed on the roof of the tunnel (along its axis) and the registration was done in the overlying rock mass (Figure 3).

The study was conducted using a modern TELSS-3 telemetric seismic station (by Geosignal Ltd., Moscow, Russia), and the first arrivals of both longitudinal and transverse elastic waves were measured as follows: the interval between the points of registration and excitation—2 m; number of registration points—76; elastic vibrations were excited by a sledgehammer weighing 6 kg. Note that the location of SRfr profiles was pre-determined by the location of the FEMR profiles where anomalous excitation of FEMR hits was registered, the technical feasibility of observations (e.g., low levels of acoustic noise), and the results of visual fracture mapping. Considering the spatial position of underground mine workings, the profile lines of SRfr measurements were carried out on straight sections with the obligatory binding of spatial coordinates by the mine surveying service. More than 800 seismic records on P- and S-waves were obtained within the framework of the research campaign. Figure 4a shows an example of the registered seismogram (Profile 2 in Table 1). All measured data were then filtered and processed. Figure 4b shows an example of the first arrivals picking diagram.

Figure 3. An example of the geophone's arrangement in the roof of a mine-working (Norilsk underground mine—Profile 2 in Table 1).

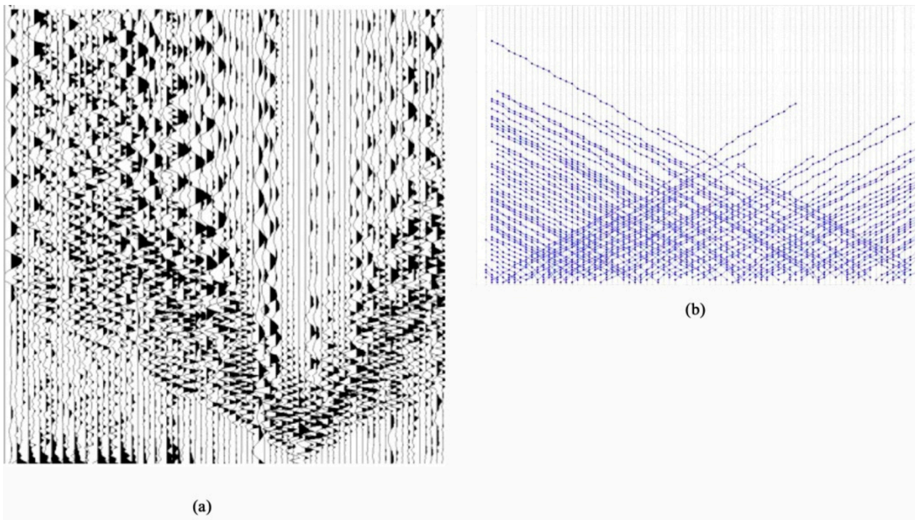

Figure 4. An example of the registered seismogram (Profile 2 in Table 1). (**a**) and the first arrivals picking (**b**).

3. Results and Discussion

Figure 5 along with Profile 2 shows the results of FEMR measurements in the underground working of the Norilsk underground mine. The anomalous values of FEMR amplitude were measured at a distance of 20–40, 80, and 120 m from the beginning of the profile (shown by black arrows in Figure 5), implying the increased stress level at this part of the mine-workings. The FEMR measurement results (Profile 2) were combined with the SRfr measurements. Figure 6 shows the results of tomographic processing of longitudinal (Vp) and transverse (Vs) wave speeds recorded at the same section of the mine-workings. Comparative analysis of Figures 5 and 6 shows a qualitative correspondence between increased FEMR amplitude and the zones of anomalously low values of P and S wave speeds at distances 20–40, 80, and 120 m from the beginning of Profile 2. The results of elastic waves processing (Vp and Vs) were used to calculate the values of Young's modulus and Poisson's ratio using well-known expressions:

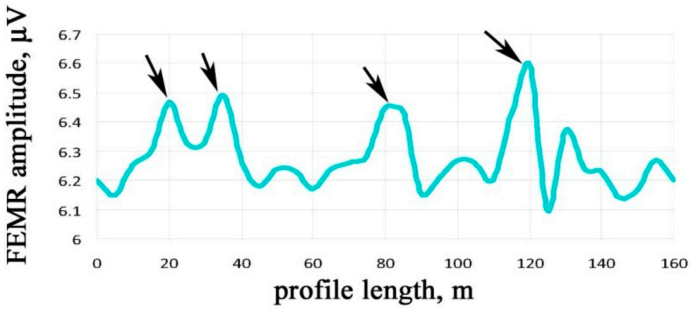

Figure 5. The results of FEMR measurement in the underground mine-workings (Profile 2). The arrows show the anomalous FEMR amplitudes.

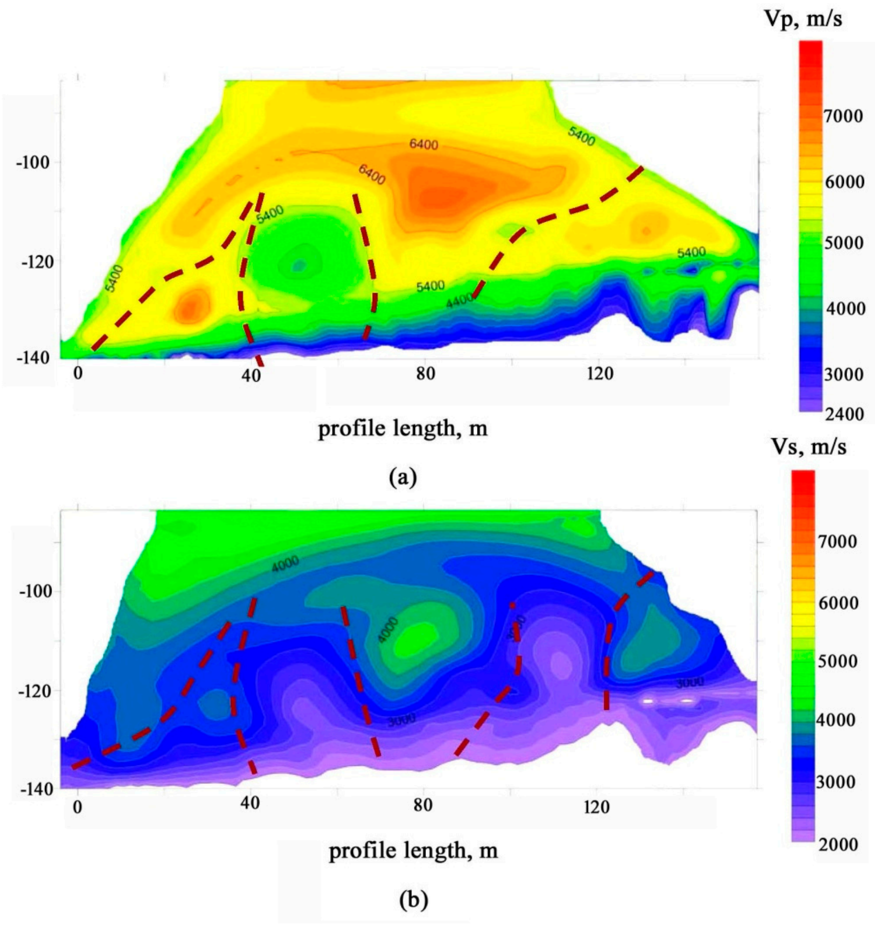

Figure 6. 2D sections obtained from SRfr measurements: compression wave speed (**a**) and shear wave speed (**b**). The dashed lines show the boundaries of anomalous zones. The *Y*-axis is the depth of measurements, the *X*-axis is the profile length (Profile 2).

$\frac{V_p}{V_s} = \sqrt{\frac{2(1-\vartheta)}{(1-2\vartheta)}}$ and $V_p = \sqrt{\frac{E}{\rho}}\sqrt{\frac{(1-\vartheta)}{(1+\vartheta)(1-2\vartheta)}}$, where ϑ is the value of Poisson's ratio, E is the value of Young's modulus, ρ is the value of rock density.

Figure 7 portrays the 2D section of these two elastic parameters. The decrease in the values of Young's modulus and increase in the value of Poisson's ratio can be interpreted as the appearance of highly fractured/weakened zones, and hence confirms the consistency of the interpretation of the increase in FEMR amplitude.

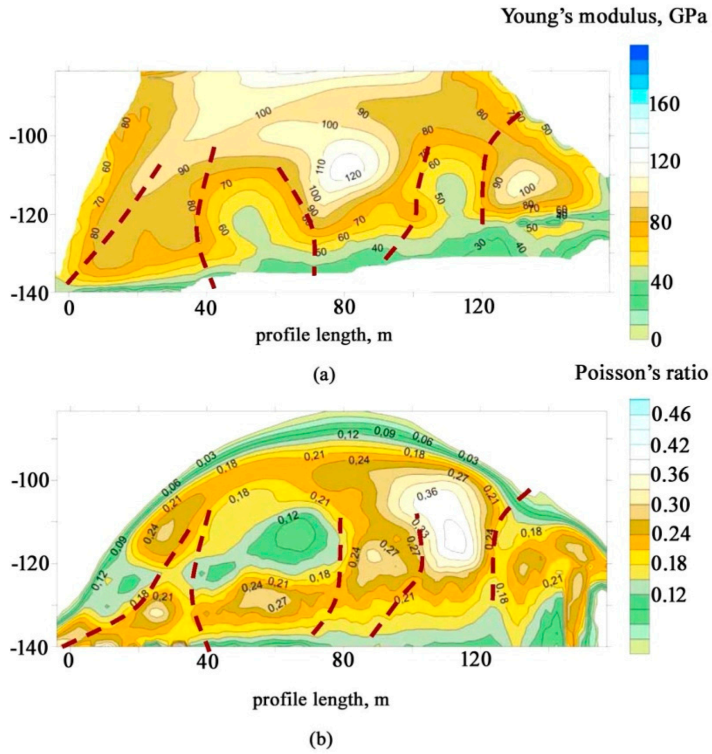

Figure 7. 2D sections of Young's modulus (**a**) and Poisson's ratio (**b**) The dashed lines show the boundaries of anomalous zones. The *Y*-axis is the depth of measurements, the *X*-axis is the profile length (Profile 2).

Figure 8 shows another example of a combined application of FEMR and SRfr methods in the zone of unstable rock mass (Profile 4 in Table 1), where Figure 8a shows the distribution of Young's modulus while Figure 8b portrays the result of FEMR registrations (Profile 4). The zone of low values of Young's modulus (marked by dashed lines) is seen at the distance of 20–50 m from the profile beginning. The same zone can be seen in Figure 8b as an anomalous value of FEMR amplitude. An appearance of both anomalies heralds the formation of highly fractured rock in the roof of the mine working and hence its potential failure.

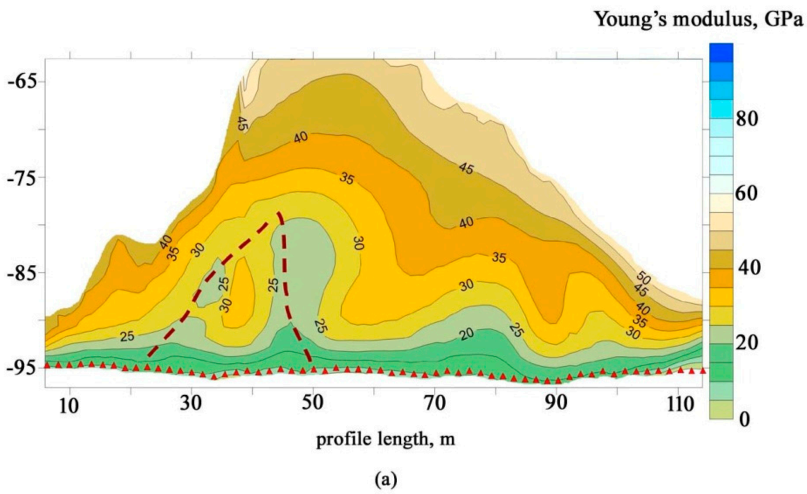

Figure 8. *Cont.*

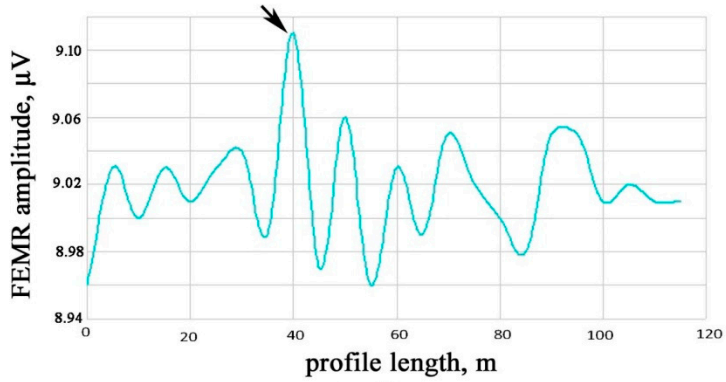

(b)

Figure 8. 2D sections of Young's modulus (**a**) and the FEMR amplitude (**b**) measured in Profile 4. The arrow in Figure 8b shows the anomalous FEMR amplitude.

4. Conclusions

The results of FEMR application in the conditions of the Norilsk underground mines show that this method can be successfully used to identify the locations of rocks which are in states of high stress or intensively fractured. However, the FEMR method allows only the estimation of the distance between zones of high stress and the surface of mine working wall or roof, and of the volume of these zones. Such a disadvantage can be overcome via the integration of FEMR measurement with the application of the SRfr method. Our study has shown that zones where elastic waves demonstrate decreased speed values of correspond with zones of increased FEMR amplitude.

That last observation can be explained as follows: the decreased speed values of elastic waves is known to be associated with a decrease in the value of Young's modulus and an increase in the value of Poisson's ratio, implying an increase in rock fracturing (rock plasticity). As it is known the fracturing of rocks is a cause of FEMR anomalies in mine working [54–59,63–65], in the laboratory during rock sample failure (e.g., [66–68]), and during earthquake nucleation (e.g., [25,69]). Hence, the coincidence of SRfr and FEMR anomalies proves the consistency of the results of this study.

The integrated application of the FEMR and SRfr methods is a preventive procedure in the framework of hazard assessment activity. When visual cracks begin to appear at the surface of the excavation roof or walls, they indicate large-scale disintegration processes [24]. Hence, conducting "preventive activity" becomes overdue and even dangerous for excavation stability and the staff activity. The presence of an overlying aquifer (as is the case in the shallow horizons of the Norilsk mines) aggravates the state of stress, and due to the activation of existing stresses, decreased friction between fracture surfaces, etc., the fracturing of the roof can cause water inflow into the excavation space and bring about its collapse.

It should be noted that the application of the SRfr method is time-consuming and labor-intensive. That is why integrating the methods is most effective approach. This should be done in a two-step manner: in the first stage, the FEMR method can be applied, enabling short-term assessment of the state of stress and hence localization of the zones where the presence of high stresses are suspected; in the second stage, the SRfr method can be used to study the state of the rocks in more detail and only in those sections of the mine-workings where increased FEMR values have been recorded.

Finally, increased FEMR amplitudes, together with low Young's modulus and high Poisson's ratio, portend unstable conditions in the roof of the underground excavation. It should be noted that the instability criteria have been developed using data accumulated in the FEMR and SRfr catalogs mentioned above, and are individual for rock type, excavation dimensions, water inflow, etc. The procedure for criteria development is a challenge for further research.

Author Contributions: Conceptualization, S.D. and N.D.; methodology, S.D. and N.D.; software, S.D. and S.M.; validation, S.D., N.D. and V.F.; formal analysis, S.D.; investigation, S.D. and N.D.; resources, S.M.; data curation, V.F.; writing—original draft preparation, S.D., N.D., V.F.; writing—review and editing, V.F.; visualization, V.F.; supervision, V.F.; project administration, S.M. All authors have read and agreed to the published version of the manuscript.

Funding: This research received no external funding.

Data Availability Statement: All data generated and analyzed during this study are included in the article.

Conflicts of Interest: The authors declare no conflict of interest.

References

1. Yakubchuk, A.; Nikishin, A. Norilsk-Talnakh Cu-Ni-PGE deposits: A revised tectonic model. *Miner. Depos.* **2004**, *39*, 125–142. [CrossRef]
2. Khramov, I.V. Maslovsky Ore Deposit of Norilsk Region: Morphology and Internal Structure of a Layered Intrusion. *Mosc. Univ. Geol. Bull.* **2010**, *65*, 134–137. [CrossRef]
3. Starostin, V.I.; Sorokhtin, O.G. A new interpretation for the origin of the Norilsk type PG-Cu-Ni sulfide deposits. *Geosci. Front.* **2011**, *2*, 583–591. [CrossRef]
4. Krivolutskaya, N.A.; Tolstykh, N.; Kedrovskaya, T.B.; Naumov, K.; Kubrakova, I.; Tyutyunnik, O.A.; Gongalsky, B.; Kovalchuk, E.N.; Magazina, L.; Bychkova, Y.V.; et al. World-Class PGE-Cu-Ni Talnakh Deposit: New Data on the Structure and Unique Mineralization of the South-Western Branch. *Minerals* **2018**, *8*, 124. [CrossRef]
5. Krivolutskaya, N.A.; Gongalsky, B.I.; Kedrovskaya, T.B.; Kubrakova, I.V.; Tyutyunnik, O.A.; Chikatueva, V.Y.; Bychkova, Y.V.; Magazina, L.; Kovalchuk, E.N.; Yakushev, A.I.; et al. Geology of the western flanks of the Oktyabr'skoe deposit, Norilsk district, Russia: Evidence of a closed magmatic system. *Miner. Depos.* **2019**, *54*, 611–630. [CrossRef]
6. Sereda, E.; Belyatsky, B.; Krivolutskaya, N. Geochemistry and Geochronology of Southern Norilsk Intrusions, SW Siberian Traps. *Minerals* **2020**, *10*, 165. [CrossRef]
7. Barnes, S.J.; Malitch, K.N.; Yudovskaya, M.A. Introduction to a Special Issue on the Norilsk-Talnakh Ni-Cu-Platinum Group Element Deposits. *Econ. Geol.* **2020**, *115*, 1157–1172. [CrossRef]
8. Freidin, A.M.; Tapsiev, A.P.; Uskov, V.A.; Nazarova, L.A.; Zaporozhtsev, A.A.; Sergunin, M.P. Re-equipment and development of mining method at Zapolyarny mine. *J. Min. Sci.* **2007**, *43*, 290–299. [CrossRef]
9. Lamzin, A.N.; Arshavskii, V.V.; Tapsiev, A.P.; Samorodov, B.N.; Zhilkina, A.F. Features of extensive deposit mining in the Oktyabrsky mine. *J. Min. Sci.* **2002**, *38*, 134–139. [CrossRef]
10. Uskov, V.A.; Eremenko, A.A.; Darbinyan, T.P.; Marysyuk, V.P. Geodynamic Hazard Assessment for Tectonic Structures in Underground Mining of North Ore Bodies in the Oktyabrsky Deposit. *J. Min. Sci.* **2019**, *55*, 77–87. [CrossRef]
11. Oparin, V.N.; Tapsiev, A.P.; Vostrikov, V.I.; Usol'tseva, O.M.; Arshavskii, V.V.; Zhilkina, A.F.; Babkin, E.A.; Samorodov, B.N.; Nagovitsyn, Y.N.; Smolov, K.V. On possible causes of the increase in seismic activity of minefields in the Oktyabrsky and Taimyrsky mines of the Norilsk deposit in 2003. Part IV: Influence of undermining of overlying rock masses. *J. Min. Sci.* **2005**, *41*, 1–5. [CrossRef]
12. Gauthier, P.T.; Blewett, T.A.; Garman, E.R.; Schlekat, C.E.; Middleton, E.T.; Suominen, E.; Crémazy, A. Environmental risk of nickel in aquatic Arctic ecosystems. *Sci. Total Environ.* **2021**, *797*, 148921. [CrossRef] [PubMed]
13. Sokolov, K.; Fedorova, L.; Fedorov, M. Prospecting and Evaluation of Underground Massive Ice by Ground-Penetrating Radar. *Geosciences* **2020**, *10*, 274. [CrossRef]
14. Kutepova, N.A. Engineering-Geological Substantiation of the Forecast of Hydro-Geomechanical Processes While Mining Operations. Ph.D. Thesis, Saint Petersburg Mining University, St. Petersburg, Russia, 2010.
15. Brady, B.; Brown, E. *Rock Mechanics for Underground Mining*; Kluwer Academic Publishers: New York, NY, USA, 2004.
16. Bacha, S.; Mu, Z.; Javed, A.; Al Faisal, S. A Review of Rock Burst's Experimental Progress, Warning, Prediction, Control, and Damage Potential Measures. *J. Min. Environ.* **2020**, *11*, 31–48. [CrossRef]
17. Bazaluk, O.; Petlovanyi, M.; Lozynskyi, V.; Zubko, S.; Sai, K.; Saik, P. Sustainable Underground Iron Ore Mining in Ukraine with Backfilling Worked-Out Area. *Sustainability* **2021**, *3*, 834. [CrossRef]
18. Oparin, V.N.; Vostrikov, V.I.; Usol'tseva, O.M.; Mulev, S.N.; Rodionova, E. Assessment of Rockburst Hazard Based on the Data of Mine Seismology. *Procedia Eng.* **2017**, *191*, 795–801. [CrossRef]
19. Hudyma, M.; Potvin, Y.H. An Engineering Approach to Seismic Risk Management in Hardrock Mines. *Rock Mech. Rock Eng.* **2010**, *43*, 891–906. [CrossRef]
20. Muraviev, E.I.; Karelin, V.N.; Shabarov, A.N. Problems and ways of developing the mineral resource base of the Polar Branch of OJSC MMC Norilsk Nickel. *Notes Min. Inst.* **2012**, *198*, 126–130.
21. Shabarov, A.N.; Kutepova, N.A.; Kutepov, Y.I. Engineering-geological security of mining operations in water-saturated massifs. *Notes Min. Inst.* **2012**, *197*, 197–202.

22. He, J.; Dou, L.; Gong, S.; Li, J.; Ma, Z. Rock burst assessment and prediction by dynamic and static stress analysis based on micro-seismic monitoring. *Int. J. Rock Mech. Min. Sci.* **2017**, *93*, 46–53. [CrossRef]
23. Cai, M.; Kaiser, P.K.; Martin, C.D. Quantification of rock mass damage in underground excavations from microseismic event monitoring. *Int. J. Rock Mech. Min. Sci.* **2001**, *38*, 1135–1145. [CrossRef]
24. Lockner, D.A.; Byerlee, J.D.; Kuksenko, V.S.; Ponomarev, A.V.; Sidorin, A. Quasi-static fault growth and shear fracture energy in granite. *Nature* **1991**, *350*, 39. [CrossRef]
25. Frid, V.; Rabinovitch, A.; Bahat, D. Earthquake forecast based on its nucleation stages and the ensuing electromagnetic radiations. *Phys. Lett. A* **2020**, *384*, 126102. [CrossRef]
26. Ding, H.-H.; Jiang, W.-W. Application of Geophysical Methods in Tunnel Exploration. In Proceedings of the 5th International Conference on Civil, Architectural and Hydraulic Engineering, Zhuhai, China, 30–31 July 2016; Atlantis Press: Zhuhai, China, 2016; pp. 188–192.
27. Li, S.; Li, S.; Zhang, Q.; Xue, Y.; Liu, B.; Su, M.; Wang, Z.; Wang, S. Predicting geological hazards during tunnel construction. *J. Rock Mech. Geotech. Eng.* **2010**, *2*, 232–242. [CrossRef]
28. Hatherly, P. Overview on the application of geophysics in coal mining. *Int. J. Coal Geol.* **2013**, *114*, 74–84. [CrossRef]
29. Fallon, G.N.; Fullagar, P.K.; Sheard, S.N. Application of geophysics in metalliferous mines. *Aust. J. Earth Sci.* **1997**, *44*, 391–409. [CrossRef]
30. Logacheva, V.M. Development of an Underground-Field Electrometric method for predicting the State of Flooded Coal-Rock Massifs of the Moscow Basin. Ph.D. Thesis, Tula State University, Tula, Russia, 2010.
31. Prostov, S.M. Substantiation and Development of Methods for Geoelectric Control of the Parameters of Fracturing and Cementation of Rocks around Workings. Ph.D. Thesis, Kemerovo State University, Kemerovo, Russia, 1996.
32. Lei, Y. Application of Geophysical Technique in the Coal Mining. *iJOE* **2015**, *11*, 11–13. [CrossRef]
33. Takahashi, T. ISRM Suggested Methods for land geophysics in rock engineering. *Int. J. Rock Mech. Min. Sci.* **2004**, *41*, 885–914. [CrossRef]
34. Takahashi, T.; Takeuchi, T.; Sassa, K. ISRM Suggested Methods for borehole geophysics in rock engineering. *Int. J. Rock Mech. Min. Sci.* **2006**, *43*, 337–368. [CrossRef]
35. Lehmann, B.; Orlowsky, D.; Misiek, R. Exploration of Tunnel Alignment using Geophysical Methods to Increase Safety for Planning and Minimizing Risk. *Rock Mech. Rock Eng.* **2010**, *43*, 105–116. [CrossRef]
36. Guy, E.D.; Nolen-Hoeksema, R.C.; Daniels, J.J.; Lefchik, T. High-resolution SH-wave seismic reflection investigations near a coal mine-related roadway collapse feature. *J. Appl. Geophys.* **2003**, *54*, 51–70. [CrossRef]
37. Isiaka, A.I.; Durrheim, R.J.; Manzi, M.S.D. High-Resolution Seismic Reflection Investigation of Subsidence and Sinkholes at an Abandoned Coal Mine Site in South Africa. *Pure Appl. Geophys.* **2019**, *176*, 1531–1548. [CrossRef]
38. Genzwill, D.J.; Brehm, R. High-resolution seismic reflections in potash mines. *Geophysics* **1993**, *58*, 741–748. [CrossRef]
39. Luxbacher, K.; Westman, E.; Swanson, P.; Karfakis, M. Three-dimensional time-lapse velocity tomography of an underground longwall panel. *Int. J. Rock Mech. Min. Sci.* **2008**, *45*, 478–485. [CrossRef]
40. Dou, L.; Chen, T.; Gong, S.; He, H.; Zhang, S. Rockburst hazard determination by using computed tomography technology in deep workface. *Saf. Sci.* **2012**, *50*, 736–740. [CrossRef]
41. Cai, W.; Dou, L.; Cao, A.; Gong, S.; Li, Z. Application of seismic velocity tomography in underground coal mines: A case study of Yima mining area Henan, China. *J. Appl. Geophys.* **2014**, *109*, 140–149. [CrossRef]
42. Cao, A.; Dou, L.; Cai, W.; Gong, S.; Liu, S.; Zhao, Y. Tomographic imaging of high seismic activities in underground island longwall face. *Arab. J. Geosci.* **2016**, *9*, 1–10. [CrossRef]
43. Czarny, R.; Pilecki, Z.; Nakata, N.; Pilecka, E.; Krawiec, K.; Harba, P.; Barnaś, M. 3D S-wave velocity imaging of a subsurface disturbed by mining using ambient seismic noise. *Eng. Geol.* **2019**, *251*, 115–127. [CrossRef]
44. Li, X.; Gong, S.; Dou, L.; Chai, Y. Detection of stress redistribution in a complex isolated coal pillar with active SVT technology. *Arab. J. Geosci.* **2020**, *13*, 1–12. [CrossRef]
45. Chlebowski, D.; Burtan, Z. Geophysical and analytical determination of overstressed zones in exploited coal seam: A case study. *Acta Geophys.* **2021**, *69*, 701–771. [CrossRef]
46. Chlebowski, D.; Burtan, Z. Mining-Induced Seismicity during Development Works in Coalbeds in the Context of Forecasts of Geomechanical Conditions. *Energies* **2021**, *14*, 6675. [CrossRef]
47. Goodfellow, S.D.; Young, R.P.A. Laboratory acoustic emission experiment under in situ conditions. *Geophys. Res. Lett.* **2014**, *41*, 3422–3430. [CrossRef]
48. Golebiowski, T.; Zogala, B.; Mendecki, M.J.; Malysa, T. The utility of rock-bolts as long electrodes for underground ERT surveys in mine-settings. *J. Appl. Geophys.* **2018**, *155*, 122–130. [CrossRef]
49. Bharti, A.K.; Prakash, A.; Verma, A.; Singh, K.K.K. Assessment of hydrological condition in strata associated with old mine working during and post-monsoon using electrical resistivity tomography: A case study. *Bull. Eng. Geol. Environ.* **2021**, *80*, 5159–5166. [CrossRef]
50. Chen, T.; Wang, X.; Mukerji, T. In situ identification of high vertical stress areas in an underground coal mine panel using seismic refraction tomography. *Int. J. Coal Geol.* **2015**, *149*, 55–66. [CrossRef]
51. Paul, A.; Mallika, V.; Murthy, S.R.; Prakash, A.; Singh, A.K. Estimation of rock load in development workings of underground coal mines a modified RMR approach. *Curr. Sci.* **2018**, *114*, 2167–2174. [CrossRef]

52. Lin, P.; Wei, P.; Wang, C.; Kang, S.; Wang, X. Effect of rock mechanical properties on electromagnetic radiation mechanism of rock fracturing. *J. Rock Mech. Geotech. Eng.* **2021**, *13*, 798–810. [CrossRef]
53. Wang, E.; He, X.; Liu, X.; Li, Z.; Wang, C.; Xiao, D. A non-contact mine pressure evaluation method by electromagnetic radiation. *J. Appl. Geophys.* **2011**, *75*, 338–344. [CrossRef]
54. Frid, V.; Vozoff, K. Electromagnetic radiation induced by mining rock failure. *Intern. J. Coal Geol.* **2005**, *64*, 57–65. [CrossRef]
55. Frid, V. Electromagnetic radiation method for rock and gas outburst forecast. *J. Appl. Geoph.* **1998**, *38*, 97–104. [CrossRef]
56. Frid, V. Rock-burst hazard forecast by electromagnetic radiation excited by rock fracture. *J. Rock Mech. Rock Eng.* **1997**, *30*, 229–236. [CrossRef]
57. Frid, V.; Shabarov, A.; Proskurjakov, V. Formation of electromagnetic radiation in coal stratum. *J. Min. Sci.* **1992**, *28*, 139–145. [CrossRef]
58. Frid, V.; Wang, E.Y.; Mulev, S.N.; Li, D.X. The Fracture Induced Electromagnetic Radiation—Approach and Protocol for the Stress State Assessment for Mining. *Geotech. Geol. Eng.* **2021**, *4*, 3285–3291. [CrossRef]
59. Frid, V.; Shabarov, A. Modern principles of nondestructive stress monitoring in mine workings—Overview. In *Eurock 2018. Geomechanics and Geodynamics of Rock Masses*; Taylor & Francis Group: London, UK, 2018; pp. 513–518. ISBN 978-1-138-61645-5.
60. Das, S.; Mallik, J.; Bandyopadhyay, K.; Das, A. Evaluation of maximum horizontal near-surface stress (SHmax) azimuth and its distribution along Narmada-Son Lineament, India by geogenic Electromagnetic Radiation (EMR) technique. *J. Geodyn.* **2020**, *133*, 101672. [CrossRef]
61. Das, S.; Mallik, J.; Dhankhar, S.; Suthar, N.; Singh, A.K.; Dutta, V.; Gupta, U. Application of Fracture Induced Electromagnetic Radiation (FEMR) technique to detect landslide-prone slip planes. *Nat. Hazards* **2020**, *101*, 505–535. [CrossRef]
62. Frid, V.; Mulev, S. Rock stress assessment based on the fracture induced electromagnetic radiation. In *Eurock 2018. Geomechanics and Geodynamics of Rock Massesl*; Taylor & Francis Group: London, UK, 2018; pp. 505–512. ISBN 978-1-138-61645-5.
63. Yakovitskaya, G.E. Development of a Method and Measuring Instruments for Diagnosing Critical States of Rocks Based on Electromagnetic Emission. Ph.D. Thesis, Novosibirsk State University, Novosibirsk, Russia, 2007.
64. Mulev, S.N.; Starnikov, V.N.; Romanevich, O.A. The current stage in the development of the geophysical method for recording natural electromagnetic radiation (EEMI). *Coal* **2019**, *10*, 1123.
65. Romanevich, K.V. Development of Criteria and Methods for Finding Geodynamic Processes by Electromagnetic Radiation Near Shallow Workings. Ph.D. Thesis, IPCON RAN, Moscow, Russia, 2015.
66. Rabinovitch, A.; Bahat, D.; Frid, V. Similarity and dissimilarity of electromagnetic radiation from carbonate rocks under compression, drilling and blasting. *Intern J. Rock Mech. Min. Sci.* **2002**, *39*, 125–129. [CrossRef]
67. Bahat, D.; Rabinovitch, A.; Frid, V. Fracture characterization of chalk in uniaxial and triaxial tests by rock mechanics, fractographic and electromagnetic methods. *J. Struct. Geol.* **2001**, *23*, 1531–1547. [CrossRef]
68. Qiu, L.; Zhu, Y.; Song, D.; He, X.; Wang, W.; Liu, Y.; Xiao, Y.; Wei, M.; Shan Yin, S.; Liu, Q. Study on the Nonlinear Characteristics of EMR and AE during Coal Splitting Tests. *Minerals* **2022**, *12*, 108. [CrossRef]
69. Contoyiannis, Y.; Potirakis, S.M.; Eftaxias, K.; Contoyianni, L. Tricritical crossover in earthquake preparation by analyzing preseismic electromagnetic emissions. *J. Geodyn.* **2015**, *84*, 40–54. [CrossRef]